



Article

# Biodegradation of Single-Walled Carbon Nanotubes in Macrophages through Respiratory Burst Modulation

Jie Hou<sup>1</sup>, Bin Wan<sup>1,\*</sup>, Yu Yang<sup>1</sup>, Xiao-Min Ren<sup>1</sup>, Liang-Hong Guo<sup>1,2,\*</sup> and Jing-Fu Liu<sup>1</sup>

<sup>1</sup> State Key Laboratory of Environmental Chemistry and Ecotoxicology, Research Center for Eco-Environmental Sciences, Chinese Academy of Sciences, Beijing 100085, China; jiehou\_st@rcees.ac.cn (J.H.); yuyang@rcees.ac.cn (Y.Y.); xmren@rcees.ac.cn (X.-M.R.); jfliu@rcees.ac.cn (J.-F.L.)

<sup>2</sup> Institute of Environment and Health, Jiangnan University, Wuhan 430056, China

\* Correspondence: binwan@rcees.ac.cn (B.W.); LHGuo@rcees.ac.cn (L.-H.G.); Tel.: +86-10-6284-9338 (B.W.); +86-10-6284-9685 (L.H.G.); Fax: +86-10-6284-9685 (L.H.G.)

Academic Editor: Vladimir Sivakov

Received: 22 February 2016; Accepted: 14 March 2016; Published: 22 March 2016

**Abstract:** The biodegradation of carbon nanotubes (CNTs) may be one of major determinants of the toxic outcomes in exposed individuals. In this study, we employed a macrophage/monocyte model, Raw264.7, to investigate the feasibility of regulating the biodegradation of three types of single-walled carbon nanotubes (SWCNTs) (pristine, ox-, and OH-SWCNTs) by respiratory burst modulation. An artificial fluid mimicking the enzymatic reactions of respiratory burst was constituted to reveal the role of respiratory burst played in SWCNT biodegradation. The biodegradation of SWCNTs were characterized by Raman, ultraviolet-visible-near-infrared spectroscopy, and transmission electron microscopy. Our results showed significantly accelerated biodegradation of ox-SWCNTs and OH-SWCNTs in macrophages activated by phorbol myristate acetate (PMA), which could be prevented by *N*-acetyl-L-cysteine (NAC), whereas p-SWCNTs were resistant to biodegradation. Similar tendencies were observed by using the *in vitro* enzymatic system, and the degradation rates of these SWCNTs are in the order of OH-SWCNTs > ox-SWCNTs >> p-SWCNTs, suggesting a pivotal role of respiratory burst in accelerating the biodegradation of SWCNTs and that defect sites on SWCNTs might be a prerequisite for the biodegradation to occur. Our findings might provide invaluable clues on the development of intervention measurements for relieving the side effects of SWCNTs and would help to design safer SWCNT products with higher biodegradability and less toxicity.

**Keywords:** single-walled carbon nanotubes; biodegradation; respiratory burst; *in vitro* enzymatic system

## 1. Introduction

Carbon nanotubes (CNTs) are one of the most important and widely used nanomaterials in research fields and consumer industrials [1,2]. Among them, functionalized single-walled carbon nanotubes (f-SWCNTs) are particularly attracting in biomedical applications [3,4], such as biomedical imaging [5], nanoinjectors [6], nanoneuroengineering [7], gene therapy [8] and drug delivery [4,9,10]. Human exposure to CNTs can potentially occur throughout the CNTs lifecycle, ranging from laboratory research, manufacturing, incorporation of CNTs into products, manipulation of CNT containing products, and finally through disposal and recycling of CNTs [11–13]. With increasing production and applications of SWCNTs, one can envision an increase of the chance of human exposure to SWCNTs and great concerns are raised on the side effects of CNTs.

Imaging and spectroscopy information unequivocally support the fact that SWCNTs can be taken up, retained, excreted or degraded within nucleated cells [14–16]. Study showed that pristine SWCNTs exposed to mice remained in the lungs for over three months [17]. Once inside organisms, the physical and chemical properties of nanomaterials usually undergo a series of alterations that either increase or reduce their toxicity. The internalized CNTs are cytotoxic [18–21], and subsequently cause pulmonary inflammation, granuloma formation and fibrosis [17,22–24] *in vivo*, mostly by inducing oxidative stress [25,26]. Reactive oxygen species (ROS)-mediated cytotoxicity can be induced by the metal impurities present in CNTs, which can be removed through CNT oxidation [27,28]. Carbon nanotubes were once considered to be resistant to chemical damage due to their rigid and perfect chemical structure, which rendered them immune to biodegradation. However, functionalized SWCNTs carrying defect sites on the sidewall and tips of the carbon nanotubes have been demonstrated to be degraded by plant-derived horse radish peroxidase (HRP) [29,30]. Thorough disintegration of the carbon nanotubes was achieved in 10 days, and oxidized aromatic fragments were detected in the course of nanotube degradation, which eventually evolved to carbon dioxide [31,32]. A study investigated the degradation of SWCNTs and MWCNTs in artificial fluids mimicking phagolysosome content and found that carboxylated SWCNTs were degraded over time along with the fracture of CNTs and disaggregation of bundles, further proving the feasibility of biodegradation of CNTs in mammalian cells [33,34]. Indeed, neutrophil myeloperoxidase (MPO) and eosinophil peroxidase (EPO) were both demonstrated to be able to degrade CNTs after supplement of exogenous H<sub>2</sub>O<sub>2</sub> [35,36]. Reactive intermediates of the peroxidase-mediated reactions were found to play an important role in the process of oxidative biodegradation of nanotubes [35–37]. Also nanotubes can be degraded by the lignin peroxidase [38] or bacteria [39], even the neutrophil extracellular traps (NETs) [40]. Most importantly, biodegraded SWCNTs did not generate an inflammatory response when aspirated into the lungs of mice [35]. Therefore, the capability of regulating the biodegradation of CNTs is of significance in modulating their toxicity.

In mammalian immune systems, polymorphonuclear neutrophils (PMN) have relatively higher level of MPO than macrophages do, and thus are more efficient in degrading CNTs [35,36]. However, it is macrophages instead of PMN cells that are more practically relevant in digesting CNTs due to: (1) PMN recruitment after SWCNT exposure is a transient rather than persistent inflammatory response, and there is no strong evidence for SWCNT phagocytosis by PMN; (2) macrophages are distributed almost throughout the body, scrutinizing for foreign particles, including nanomaterials, so that they have better chance of encountering and engulfing CNTs; (3) there are multiple evidences showing that CNTs resident in tissues including lung and brain were engulfed by macrophages [41–43]. Fortunately, monocytes/macrophages can be activated as they come into contact with bacteria or fungi, and the oxygen consumption increases significantly along with the rapid generation of reactive oxygen species (superoxide radicals and hydrogen peroxide) [35,38] to degrade internalized particles and bacteria, which is defined as respiratory burst [44]. The whole reaction is initiated with the activation of nicotinamide adenine dinucleotide phosphate (NADPH)-oxidase that reduces O<sub>2</sub> to superoxide anion (O<sub>2</sub><sup>•−</sup>), which is then catalyzed by superoxide dismutase (SOD) to form H<sub>2</sub>O<sub>2</sub>. Myeloperoxidase (MPO) further combines H<sub>2</sub>O<sub>2</sub> with Cl<sup>−</sup> to produce hypochlorite, which plays a role in destroying bacteria as well as internalized particles such as SWCNTs [35,44,45]. Chemicals such as lipopolysaccharide (LPS), PMA, are known to initiate the respiratory burst in macrophages, and thus provide a meaningful way to modulate the biodegradation of CNTs.

In this study, we employed a macrophage/monocyte model, Raw264.7 cells, to investigate the feasibility of controlling the biodegradation of SWCNTs, by either respiratory burst inducer or the anti-oxidant treatment. In addition, an artificial fluid was constructed to simulate the enzymatic reactions of respiratory burst to reveal the role of respiratory burst played in the SWCNT biodegradation. Simultaneously, different SWCNTs (pristine, acid oxidized and hydroxylated SWCNTs) were used to study the influence of functional surface groups on the biodegradation of SWCNTs. The results showed that stimulation of respiratory bursts in macrophages could accelerate

the degradation of SWCNTs significantly, while anti-oxidant treatment inhibited the process. Pristine SWCNTs were resistant to degradation, whereas acid oxidized and hydroxylated SWCNTs were degraded upon respiratory bursts, indicating that functionalization of SWCNTs introducing defect sites is a prerequisite for CNT degradation.

## 2. Results

### 2.1. Characterization of Single-Walled Carbon Nanotubes (SWCNTs)

The characterization of SWCNTs by transmission electron microscopy (TEM) showed that pristine SWCNTs (p-SWCNTs), acid-oxidized SWCNTs (ox-SWCNTs), and hydroxylated SWCNTs (OH-SWCNTs) all presented as fibrillar shape and retained the structural integrity of carbon nanotubes (Figure 1A). Fourier transform infrared spectroscopy (FT-IR) analyses on these SWCNTs showed the presence of carboxyl groups ( $\nu = 1635 \text{ cm}^{-1}$ ,  $-\text{COOH}$ ) and hydroxyl groups ( $\nu = 3433 \text{ cm}^{-1}$ ,  $-\text{OH}$ ) on the surface of ox-SWCNTs, while only hydroxyl groups ( $\nu = 3234 \text{ cm}^{-1}$ ,  $-\text{OH}$ ) were present on the surface of OH-SWCNTs and no functional group was found on the surface of p-SWCNTs (Figure 1B). In the Raman spectrum, the two characteristic peaks: disorder induced D-band at  $\sim 1340 \text{ cm}^{-1}$  ( $\pm 10$ ) and tangential mode G-band at  $\sim 1580 \text{ cm}^{-1}$  ( $\pm 10$ ) were identified and  $I_D/I_G$  ratios were shown as insets (Figure 1C) in the order of: OH-SWCNTs ( $I_D/I_G = 0.46$ ) > ox-SWCNTs (0.33) > p-SWCNTs (0.09). The diameters and length of these SWCNTs were listed in supplementary Table S1.

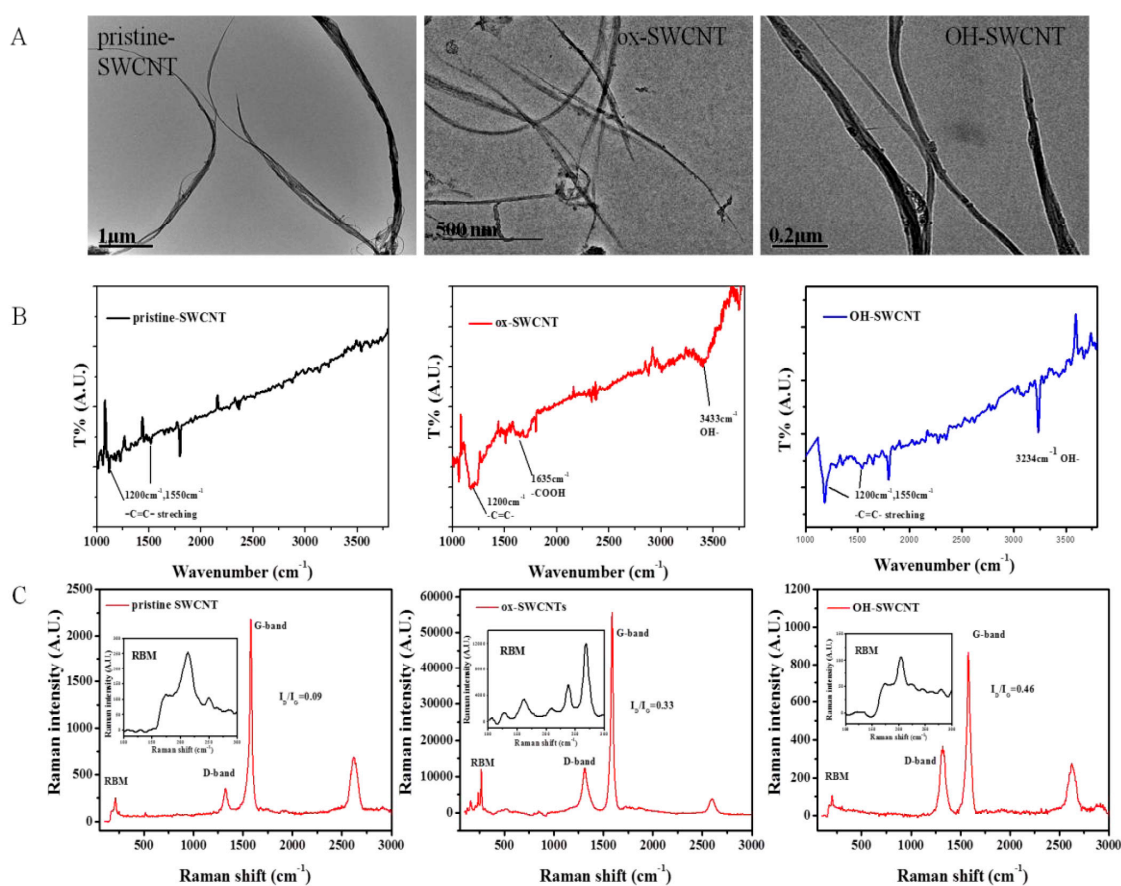


**Figure 1.** Characterization of three types of SWCNTs: (A) TEM images of (from left to right) pristine-SWCNTs, ox-SWCNTs, and OH-SWCNTs; (B) FT-IR spectra of (from left to right) pristine-SWCNTs, ox-SWCNTs, and OH-SWCNTs, showing the presence of  $-\text{C}=\text{C}-$  stretching ( $\nu = 1200$  and  $1550 \text{ cm}^{-1}$ ),  $-\text{COOH}$  ( $\nu = 1635 \text{ cm}^{-1}$ ) and  $-\text{OH}$  ( $\nu = 3200\text{--}3600 \text{ cm}^{-1}$ ) [46–48]; (C) Raman spectra of (from left to right) pristine-SWCNTs, ox-SWCNTs, and OH-SWCNTs. G-band and D-band were indicated.  $I_D/I_G$  ratios were shown as insets.

## 2.2. Biodegradation of SWCNTs in Macrophages

### 2.2.1. Induction of Respiratory Burst in Macrophages

The respiratory burst can be activated through the interaction between macrophages and microorganisms or by other stimuli including chemotactic factors and phorbol esters such as phorbol myristate acetate (PMA) [49–51]. In this study, we used PMA as the activator to induce respiratory burst in macrophages, and the anti-oxidant, *N*-acetyl-L-cysteine (NAC), as the inhibitor of the respiratory burst. The respiratory burst was evaluated through the measurement of reactive oxygen species (ROS) generation by using a 2',7'-dichlorofluorescein diacetate (DCF-DA) assay. When cells were treated with different concentrations of PMA (0–2  $\mu$ M), the fluorescence of intracellular DCF increased over time and 0.5  $\mu$ M PMA has the highest intensity of DCF fluorescence, indicating the maximum generation of ROS and respiratory burst in macrophages under this treatment (Figure 2A). We further optimized the concentration of NAC pretreatment for inhibiting the respiratory burst. The results showed that NAC pretreatment could significantly inhibit the ROS production in a concentration-dependent manner (Figure 2B). One mM NAC pretreatment was selected for further experiments. In addition, the effects of PMA and NAC on the generation of ROS in macrophages were observed by direct imaging of DCF fluorescence signals in cells and are shown in Figure 2C.

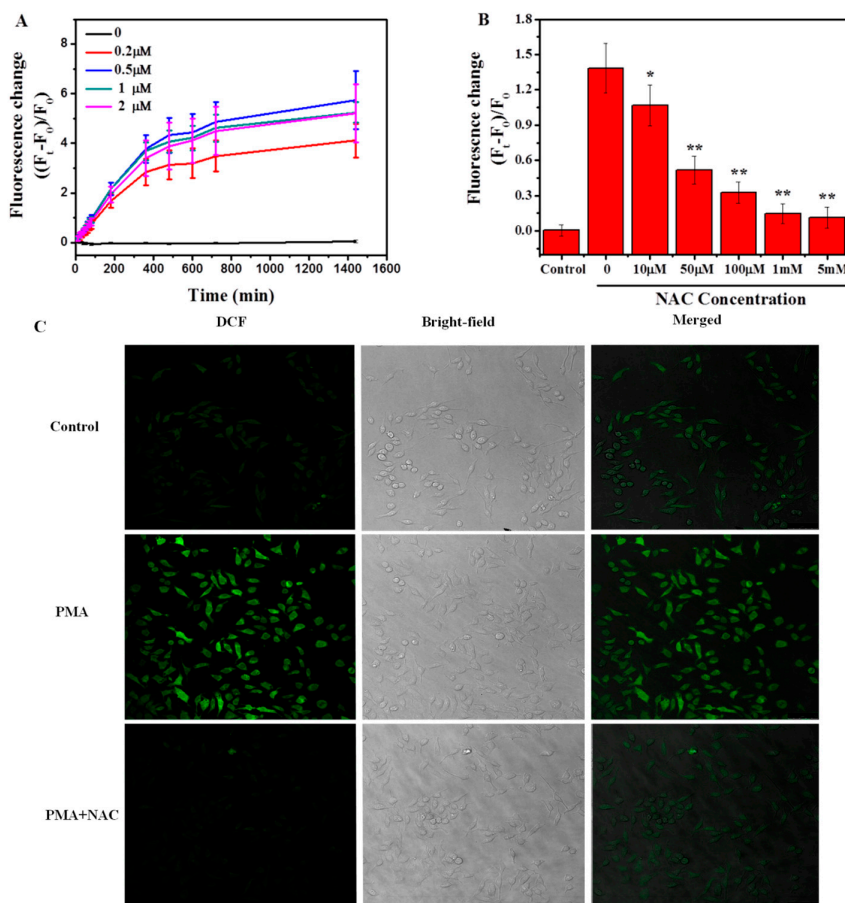


**Figure 2.** Induction and inhibition of respiratory burst in macrophages by PMA and NAC, respectively, evaluated through the generation of ROS. (A) Fluorescence intensity change of DCF over time in macrophages under the treatment of 0–2  $\mu$ M PMA; (B) Fluorescence intensity change of DCF in macrophages with different concentrations of NAC pretreatment, followed by 0.5  $\mu$ M PMA stimulation for 3 h (Ft); (C) Representative confocal images of macrophages treated in (B) with PMA concentration 0.5  $\mu$ M, and NAC 1 mM. Green fluorescence represents DCF signal. The control group was cells without any treatment. Scale bar = 50  $\mu$ M. (\*  $p < 0.05$ ; \*\*  $p < 0.01$ ).

### 2.2.2. Characterization of SWCNTs Degradation in Macrophages

On the basis of the respiratory burst model, we exposed the macrophages to different types of SWCNTs and observed the degradation of these SWCNTs by using transmission electron microscopy (TEM), ultraviolet-visible-near-infrared (UV-vis-NIR) spectroscopy, and Raman spectroscopy [31]. The optical absorption of carbon nanotubes is a quick and facile method to obtain the information of nanotubes [52]. Because the SWCNTs are usually synthesized in the format of mixtures with various chiralities and diameters, they possess metallic and semiconducting properties. Since respiratory burst takes place mainly inside of cells, CNTs must be internalized first before degradation occurs, as evidenced in the present study (Figure S1). The treatment of p-SWCNTs, ox-SWCNTs, and OH-SWCNTs (5  $\mu\text{g}/\text{mL}$ ) in the presence or absence of PMA (0.5  $\mu\text{M}$ ) did not cause cell viability loss (Figure S2). In this study, we observed the typical UV-vis-NIR spectra of carbon nanotubes, showing the characteristic metallic band ( $M_1$ ,  $\sim 900\text{--}1000$  nm) and semiconducting transition absorbing band ( $S_2$ ,  $\sim 1100\text{--}1200$  nm) [53] (Figure 3A,D,G). The transitions related to the  $sp^2$ - carbon framework of the SWCNTs will lessen when the oxidation of the graphitic structure occurs, and decreased absorbance of the band would indicate the degradation of carbon nanotubes [32]. We found a decrease in the absorbance of the metallic, especially the semiconducting band of SWCNTs in macrophages treated with PMA (Figure 3E,H, red lines), compared to those in untreated macrophages (black lines). After normalization against baseline and through the peak area calculation, we quantitatively detected the significant decrease in  $S_2$  band of ox- and OH-SWCNTs in PMA-treated macrophages (Figure 3F,I), suggesting different degrees of degradation of both SWCNTs. Interestingly, when cells were pretreated with 1 mM NAC, followed by PMA stimulation, the decreased absorbance of  $S_2$  band was alleviated significantly for OH-SWCNTs, and the even the absorbance was increased for ox-SWCNTs (Figure 3E,H, blue line), suggesting that anti-oxidant could inhibit the degradation of SWCNTs. No increase or decrease of either  $M_1$  or  $S_2$  band absorbance was observed for p-SWCNTs (Figure 3B,C), suggesting that p-SWCNTs are resistant to the biodegradation by cells, even when macrophages were in respiratory burst.

The damage of SWCNT structure was also characterized by Raman microscopy (Figure 4), which allows monitoring the evolution of the oxidation of the SWCNTs [33]. Compared to their corresponding original SWCNTs, ox-SWCNTs and OH-SWCNTs showed increased intensity of disorder induced D-band at  $\sim 1340$   $\text{cm}^{-1}$  ( $\pm 10$ ) whereas the tangential mode G-band at  $\sim 1580$   $\text{cm}^{-1}$  ( $\pm 10$ ) was decreased in untreated macrophages, indicating the oxidation damage on the graphene walls and the resulting of  $I_D/I_G$  ratios were increased from 0.33 to 0.63 ( $\pm 0.02$ ) for ox-SWCNTs, and from 0.46 to 0.53 ( $\pm 0.05$ ) for OH-SWCNTs (Figure 1C vs. Figure 4D; Figure 1C vs. Figure 4F). These data suggested that macrophages could normally degrade ox- and OH-SWCNTs. When macrophages were stimulated with PMA, the increase of  $I_D/I_G$  ratios was even prominent after 24 h, from 0.33 to 0.81 ( $\pm 0.04$ ) for ox-SWCNTs (Figures 1C and 4D) and from 0.46 to 0.73 ( $\pm 0.07$ ) for OH-SWCNTs (Figures 1C and 4F). The results suggested that PMA-induced respiratory burst in macrophages could accelerate the biodegradation of ox- and OH-SWCNTs, inducing more defect sites on SWCNTs. Meanwhile, we found that NAC pretreatment of cells could significantly attenuate the biodegradation of ox-SWCNTs and OH-SWCNTs, with the  $I_D/I_G$  ratios returned to control levels (Figure 4D,F). No above-mentioned effect was observed for p-SWCNTs. Taken together, our data support that macrophages can normally degrade ox-SWCNTs and OH-SWCNTs and the process can be speeded up significantly by PMA-induced respiratory burst in macrophages, probably through the generation of large amount of ROS, and thus anti-oxidant treatment with NAC can efficiently block the process.

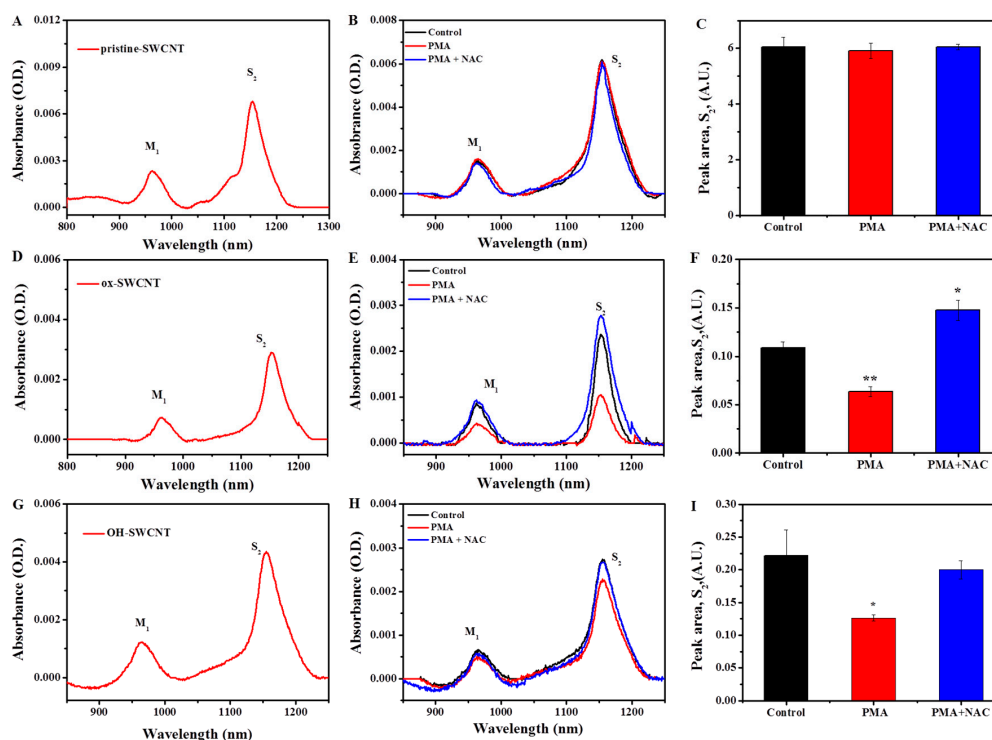


**Figure 3.** Biodegradation of SWCNTs in macrophages for 24 h with or without PMA activation, as evaluated by the infrared (NIR) spectra, normalized against baseline. (A,D,G) Typical UV-vis-NIR spectra of p-SWCNTs, ox-SWCNTs and OH-SWCNTs, respectively; (B,E,H) Influence of PMA and NAC treatment on the absorbance of  $M_1$  and  $S_2$  bands of p-SWCNTs, ox-SWCNTs and OH-SWCNTs in macrophages, respectively. Black line: control macrophages (untreated); Red line: PMA-activated macrophages; Blue line: PMA-activated macrophages with NAC pretreatment; (C,F,I) Quantification of the peak area of characteristic semiconducting transition band ( $S_2$ ) of (C) p-SWCNTs; (F) ox-SWCNTs; and (I) OH-SWCNTs in macrophages. Results were from at least three independent experiments and expressed as mean  $\pm$  S.D. (\*  $p < 0.05$ ; \*\*  $p < 0.01$ ).

### 2.3. Biodegradation of SWCNTs in Respiratory Burst Enzymatic System *in Vitro*

To further confirm the role of respiratory burst in the degradation of SWCNTs, we constructed an enzymatic system to simulate the respiratory burst *in vitro* [54–56]. Respiratory burst is initiated by the activation of NOX (NADPH Oxidase), which is a complex enzyme consisting of five components including  $p40^{PHOX}$  (PHOX for Phagocyte oxidase),  $p47^{PHOX}$ ,  $p67^{PHOX}$ ,  $p22^{PHOX}$  and  $gp91^{PHOX}$ . Once the cell is activated, the cytosolic subunits migrate to the membrane, where they bind to cytochrome b558 to assemble the active oxidase [57–59]. NOX catalyzes the generation of  $O_2^{\bullet-}$  from NADPH by transferring an electron to oxygen. Then the  $O_2^{\bullet-}$  is converted to  $H_2O_2$  by superoxide dismutase (SOD). And the  $H_2O_2$  serves as the substrate for peroxidase such as MPO in oxidating halides to generate hypohalous acids [44,60]. First, the construction of *in vitro* respiratory burst enzymatic reaction was evaluated by the measurement of  $O_2^{\bullet-}$  to test the activity of NOX. The NOX solution itself could not generate detectable amount of  $O_2^{\bullet-}$ , manifested as constant low level of the absorption of ferrocyanide at 550 nm (Figure 5A). However, the absorption of ferrocyanide increased over time after the addition of NADPH into the NOX solution, and the increase could be significantly inhibited by SOD (100 U/mL), suggesting that NOX was viable to produce  $O_2^{\bullet-}$  after supplement of NADPH (Figure 5A). Next, we optimized the concentration of NADPH by measuring the production of  $H_2O_2$  in the NOX + SOD system supplemented with different concentrations of NADPH, and results showed that addition of 5 mM NADPH generated the maximum amount of  $H_2O_2$  (Figure 5B). The data indicated that the *in vitro* respiratory burst enzymatic system was constructed successfully and could generate required substrates ( $H_2O_2$ ) for MPO.

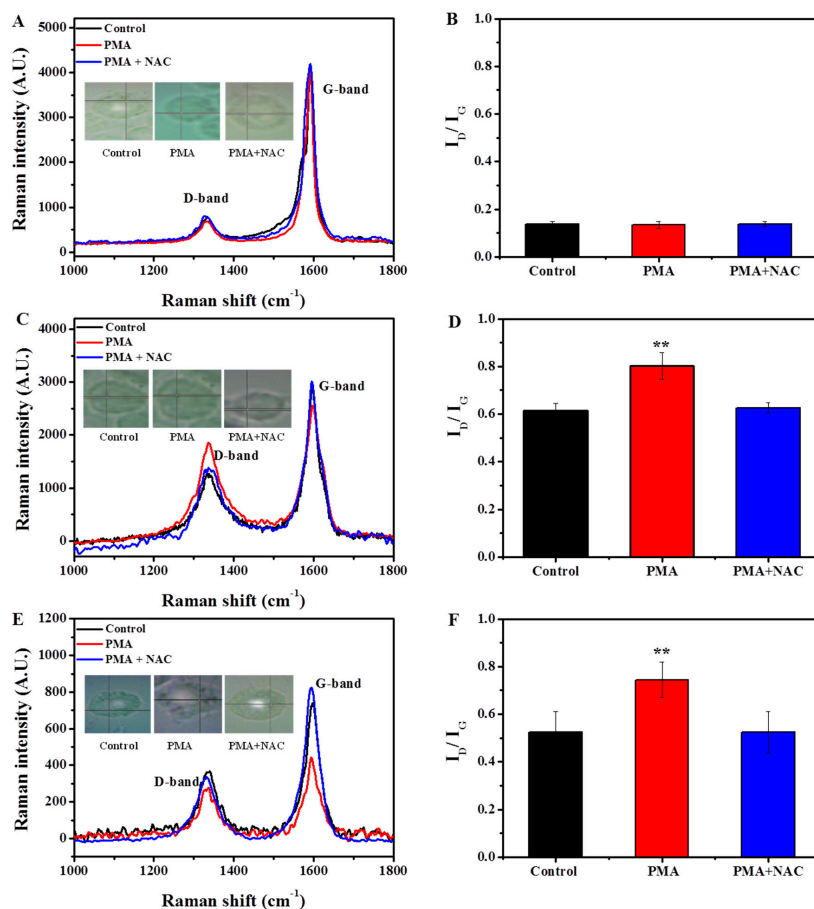


**Figure 4.** Biodegradation of SWCNTs by macrophages for 24 h, as characterized with Raman spectra. (A,C,E) Representative Raman spectra of p-SWCNTs, ox-SWCNTs, and OH-SWCNTs incubated with un-stimulated macrophages (control, black line), PMA-activated macrophages (PMA, red line), and PMA-activated macrophages with NAC treatment (PMA + NAC, blue line) for 24 h. Corresponding cell images and sampling sites were shown as insets; (B,D,F) Quantitative  $I_D/I_G$  ratios of p-SWCNTs, ox-SWCNTs, and OH-SWCNTs treated in (A,C,E), respectively. The results were obtained from at least 20 spectra and expressed as mean  $\pm$  S.D. (standard deviation). (\*\*  $p < 0.01$ ).

The nanotubes were previously shown to be degraded by hMPO in the presence of  $H_2O_2$  [35,37,61]. hMPO can catalyze the production of even stronger oxidizing substances such as hypohalous acids in the presence of sodium chloride (NaCl) to degrade internalized particles and bacteria [44]. We therefore incubated SWCNTs in the *in vitro* enzymatic system with the addition of NaCl, and at different time points (8, 24, and 30 h) we sampled the SWCNTs to track the degradation process of SWCNTs. As shown in Figure 6, for p-SWCNTs, the Raman spectra have little or no change in the D-band and G-band intensity in MPO only, full enzyme solution (MPO + SOD + NOX) and NAC (MPO + SOD + NOX + NAC) groups, which means there is nearly no oxidation on p-SWCNTs. As for ox-SWCNTs and OH-SWCNTs, MPO alone caused no change in the Raman spectra, but in full enzyme solution, both types of SWCNTs exhibited the tendency of degradation as  $I_D/I_G$  ratios increased with time (Figure 6, ox-SWCNTs, OH-SWCNTs), to 0.67 ( $\pm 0.05$ ) and 0.85 ( $\pm 0.04$ ) for ox-SWCNTs at 24 and 30 h, respectively, and to 0.76 ( $\pm 0.04$ ) and 0.93 ( $\pm 0.06$ ) for OH-SWCNTs at 24 and 30 h, respectively, suggesting that defect sites of SWCNTs increased and the structure of nanotubes were damaged. However, the degradation process could be suppressed by the addition of NAC to the full enzyme solution, as shown in Figure 6 (MPO + SOD + NOX + NAC group), proving that SWCNT biodegradation induced by respiratory burst could be completely inhibited (OH-SWCNTs) or alleviated (ox-SWCNTs) by anti-oxidants that scavenge the ROS.

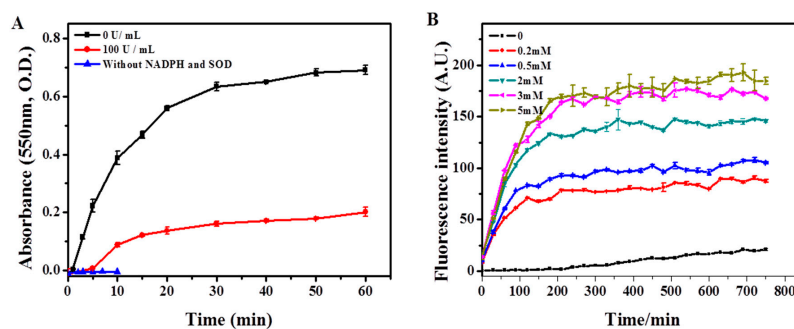


**Figure 5.** Construction of the *in vitro* respiratory burst enzymatic system, as evaluated through the generation of  $O_2^{*-}$  and  $H_2O_2$ . (A) The generation of  $O_2^{*-}$  by NOX solution over time in the presence or absence of SOD, as measured by ferrocytochrome c absorbance at 550 nm; (B) The production of  $H_2O_2$  over time by NOX and SOD catalyses, in the presence of different concentrations (0–5 mM) of NADPH, as measured by the fluorimetric hydrogen peroxide assay. The data demonstrated that NOX was viable to produce  $O_2^{*-}$ , which was then converted to  $H_2O_2$  by SOD.

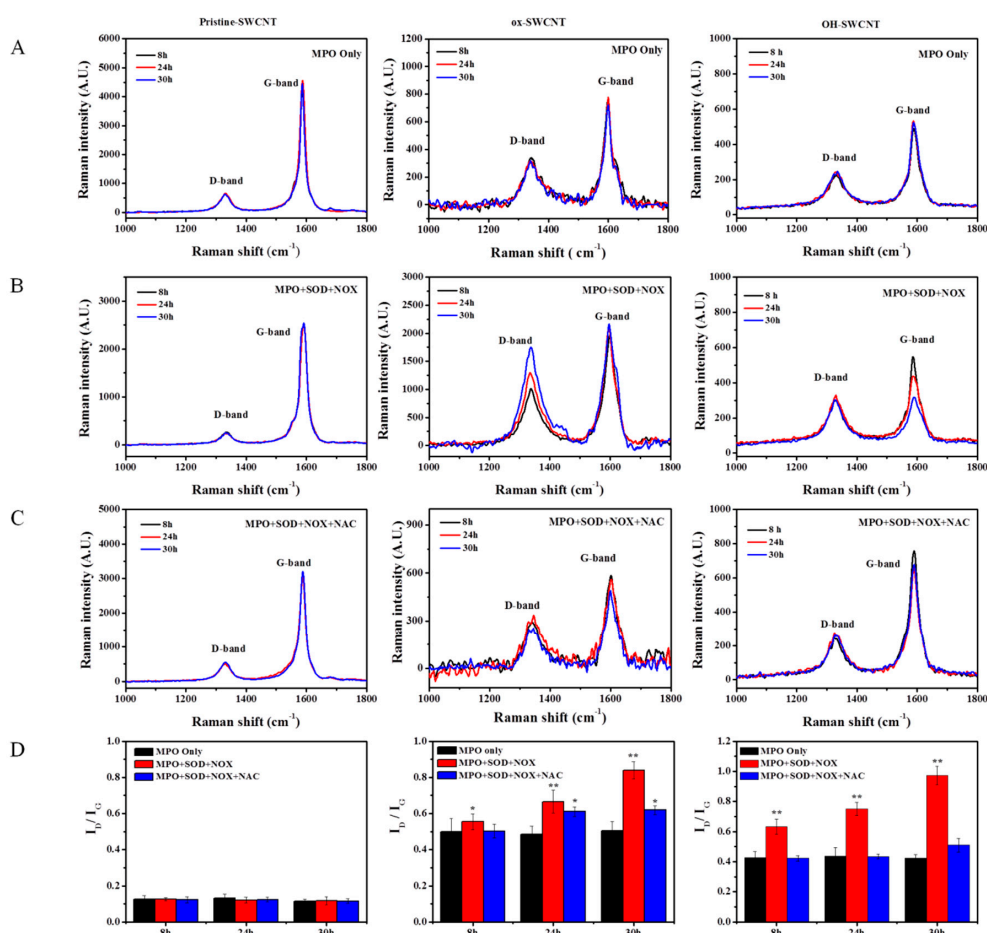


**Figure 6.** Degradation of SWCNTs by *in vitro* respiratory burst enzymatic system, as measured by Raman spectra. Column from left to right: pristine-SWCNTs, ox-SWCNTs and OH-SWCNTs (8  $\mu$ g per sample). (A) Raman spectra of SWCNTs incubated with MPO alone (containing 140 mM NaCl, 1 U MPO, and 1 mM EGTA in PBS buffer) for the indicated time; (B) Raman spectra of SWCNTs incubated in full enzyme solution (labeled as MPO + SOD + NOX) for indicated time; (C) Raman spectra of SWCNTs in full enzyme solution supplemented with 1 mM NAC (labeled as MPO + SOD + NOX + NAC); (D) Corresponding quantitative measurement of  $I_D/I_G$  ratios of SWCNTs incubated in (A–C). Results shown are the mean values  $\pm$  S.D. of at least 20 spectra. Significance of differences by comparing with MPO only group was indicated with asterisks (\*  $p < 0.05$ ; \*\*  $p < 0.01$ ).

We further used UV-vis-NIR spectroscopy to assess the degradation of SWCNTs after 24 and 30 h incubation with enzyme solutions (Figure 7). Very similar to the results obtained from Raman spectrum analyses, we found essentially no change in the absorbance of  $S_2$  band of p-SWCNTs (Figure 7, pristine-SWCNTs). However, both ox-SWCNTs and OH-SWCNTs showed a significant decrease of the absorbance of  $S_2$  band in a time-dependent manner after being incubated with full enzyme solution, whereas the addition of NAC significantly inhibited the degradation process, with the peak area of  $S_2$  band back to the level comparable to that of MPO alone group (Figure 7C).

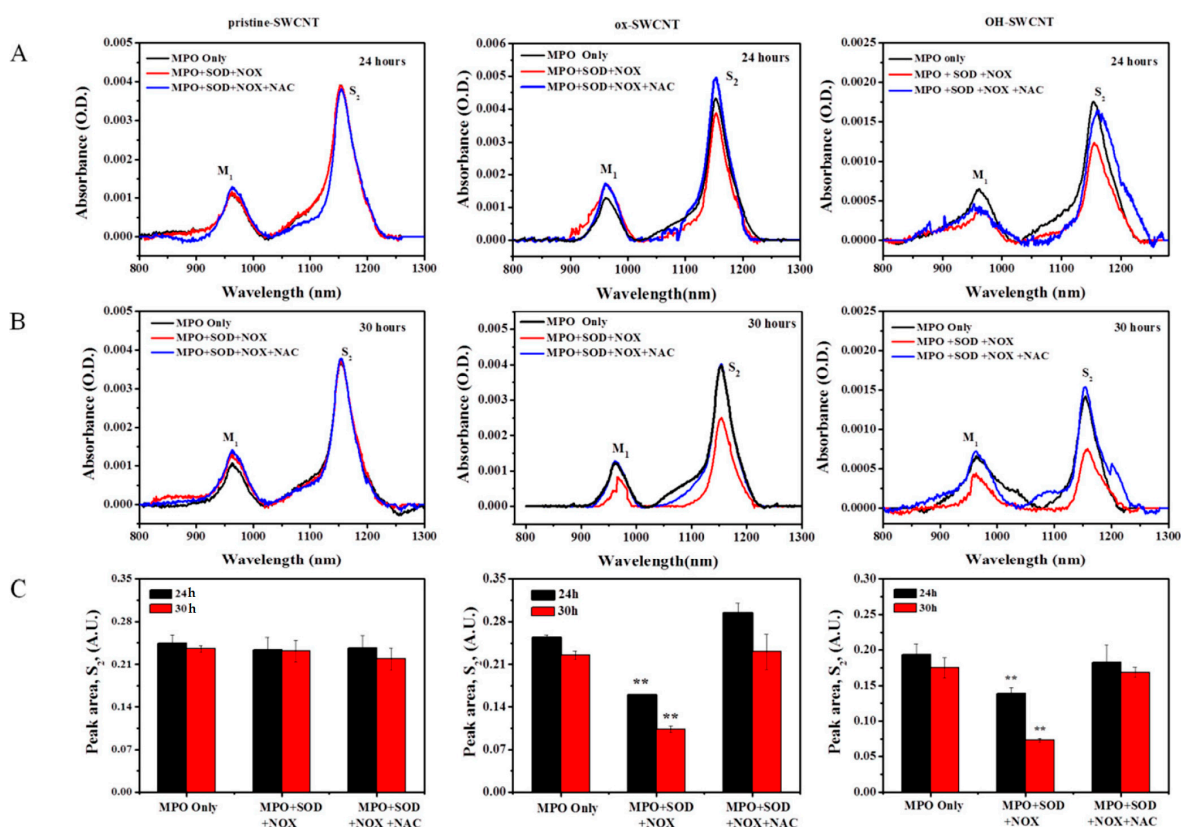


**Figure 7.** Degradation of SWCNTs by *in vitro* respiratory burst enzymatic system, as measured by UV-vis-NIR, normalized against baseline. Column from left to right: pristine-SWCNTs, ox-SWCNTs and OH-SWCNTs. The UV-vis-NIR spectra of SWCNTs incubated for 24 h (A) and 30 h (B) with different solutions were shown; (C) The peak area of  $S_2$  spectra of SWCNT. The reduced intensity of the  $S_2$  absorbance spectra indicating the degradation of SWCNTs. Results were from at least three samples and expressed as mean  $\pm$  S.D. Significance of differences by comparing with the MPO only group was indicated with asterisks (\*\*  $p < 0.01$ ).

The relatively simple composition of an *in vitro* enzymatic system allows us to examine the morphological change of SWCNTs as a result of enzymatic degradation by using transmission electron microscopy (TEM) (Figure 8). Before incubation in the enzymatic system, all original SWCNTs samples appeared to have a fiber-like shape, as shown in Figure 1. After 24 h incubation, no morphological change was observed for p-SWCNTs, which still exist as long-fiber shaped tubes (Figure 8, pristine-SWCNTs). For ox-SWCNTs and OH-SWCNTs, MPO treatment alone did not induce apparent change of SWCNTs, whereas in full enzyme solution, both SWCNTs underwent serious structural damage, resulting in fragmentation and loss of fibrous structure. Most of the tubular structure of SWCNTs became undefined. In addition, a small amount of debris and pieces of nanotubes were observed (Figure 8B). Taken together, our data obtained using an *in vitro* respiratory burst enzymatic system suggests that MPO alone could barely degrade SWCNTs; full respiratory

burst enzymatic system could only degrade the ox-SWCNTs and OH-SWCNTs but not p-SWCNTs. More importantly, the degradation process can be modulated by NAC.

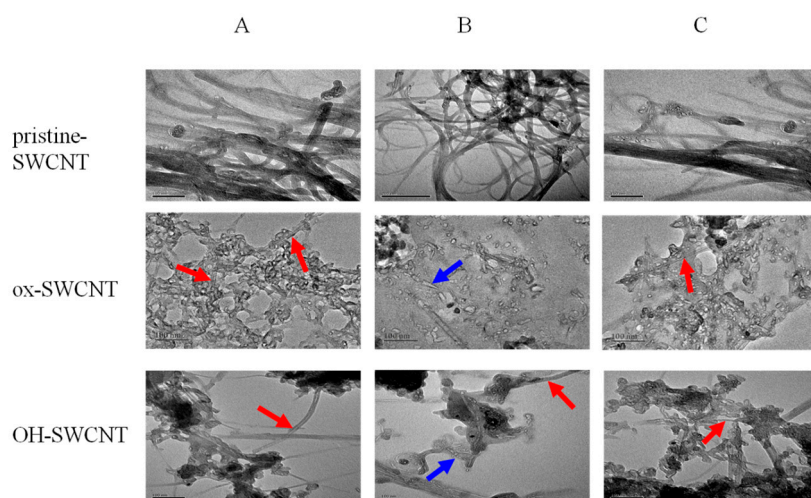


**Figure 8.** TEM imaging of SWCNTs (pristine-SWCNT, ox-SWCNT, OH-SWCNT) after 24 h incubation with *in vitro* respiratory burst enzymatic system. (A) MPO only; (B) Full enzyme solution (MPO + SOD + NOX); (C) Full enzyme solution supplemented with 1 mM NAC. Red arrows point to SWCNTs with long fiber-like shape; Blue arrows point to degraded fragments of SWCNTs. Scale bar = 100 nm.

### 3. Discussion

The biodegradability of carbon nanotubes may be a major determinant of the toxic outcomes in exposed individuals [35]. Peroxidases such as MPO and EPO have been demonstrated to be able to degrade SWCNTs [35,36], due to their capability of converting  $H_2O_2$  and oxidating halides to generate hypohalous acids [59,60,62]. In mammalian systems, macrophages are ubiquitous, patrolling for invading pathogens, dying cells and particles. Most often CNTs exposed to individuals were found engulfed by macrophages [41]. Thus, macrophages constitute the potential target cells for modulating CNTs biodegradation. The respiratory burst in macrophages activates a series of enzymatic reactions involving the enzyme NADPH oxidase, SOD (Cu/ZnSOD and MnSOD), and MPO that ultimately produce hypochlorous acid (HClO). Therefore, activation of respiratory bursts in macrophages by PMA would accelerate the biodegradation of internalized SWCNTs, as shown in this study. More prominently, our results also demonstrated that due to the intrinsic property of ROS production during the respiratory burst, an anti-oxidant treatment (such as NAC) of cells could efficiently suppress the degradation process.

Recently, the reactive intermediate produced by respiratory burst,  $O_2^{*-}$ , was also shown to react with nitric oxide ( $NO^*$ ) to generate a potent oxidant-peroxynitrite ( $ONOO^-$ ), which plays an important role in macrophage biodegradation of SWCNTs [63]. Therefore, PMA-induced respiratory burst in macrophages may also activate the peroxynitrite-driven biodegradation of SWCNTs. To further confirm the role of respiratory burst in the biodegradation of SWCNTs, we constructed an *in vitro* simulating enzymatic fluid of respiratory burst to rule out the interference of peroxynitrite. The simulating fluid could generate sufficient amounts of reactive intermediates including  $O_2^{*-}$  and  $H_2O_2$  (Figure 5), to provide substrates for MPO. Very similar to the results obtained from PMA-activated macrophages, the *in vitro* system containing full enzymes could considerably degrade ox-SWCNTs and OH-SWCNTs, manifested as increased  $I_D/I_G$  ratios and decrease of  $S_2$  band. In addition, NAC supplemented to the system could cause apparent inhibition of the biodegradation of SWCNTs. These data suggested that respiratory burst played an important role in the biodegradation of SWCNTs, and the *in vitro* enzymatic system might be a useful tool to simulate the respiratory burst for other applications.

Previous studies showed a close relationship between the surface chemistry and the biodegradation of CNTs, and it seems that carboxylation on CNT surface is a prerequisite for CNT degradation [35]. The possible reason is because the carboxylation on CNTs might break the  $\pi$ - $\pi$  interactions of CNTs and create two reactive sites that are potential sites for oxidative attack [64]. In this study, we compared three types of SWCNTs with different surface modifications, including p-SWCNTs, ox-SWCNTs, and OH-SWCNTs. The infrared spectra assessments revealed about 51% of OH-SWCNTs and 25% of ox-SWCNTs were degraded after 8 h incubation with an *in vitro* enzymatic system. After 30 h incubation, 63% of OH-SWCNTs and 53% of ox-SWCNTs were degraded. During the whole incubation, only negligible degradation (<5%) of pristine SWCNTs was observed (Figure 9). This suggests that except for p-SWCNTs carrying negligible defect sites, both ox-SWCNTs and OH-SWCNTs underwent serious structural damage and OH-SWCNTs were more susceptible to the oxidative attack than ox-SWCNTs. During the preparation of ox-SWCNTs, the acid oxidation of SWCNTs introduced both carboxyl and hydroxyl groups on the surface of SWCNTs, while OH-SWCNTs possess hydroxyl groups only (Figure 1B). It is difficult to differentiate the contribution of the carboxyl and hydroxyl groups to the biodegradation of SWCNTs. However, our results at least illustrated that oxygen-functionalized SWCNTs were biodegradable. Alternatively, the higher biodegradation of OH-SWCNTs may result from the fact that OH-SWCNTs originally possess higher level of defect sites than ox-SWCNTs do (Figure 1C), and thus provide more points for oxidative attack.

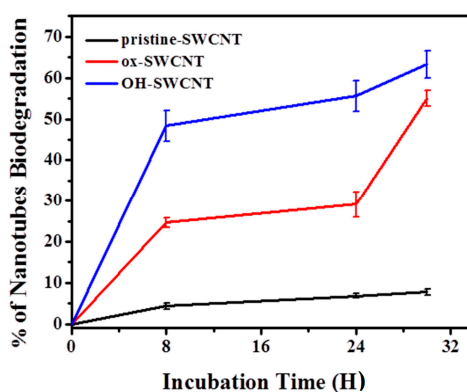


**Figure 9.** Biodegradation of SWCNTs by *in vitro* enzymatic system over time. The level of biodegradation at different time points is plotted as percentage assessed by the intensity magnitudes of the characteristic semi-conducting ( $S_2$ ) peaks of SWCNTs present in the recorded Vis-NIR spectra.

We observed 27% degradation of ox-SWCNTs after 24 h incubation with the *in vitro* enzymatic system (Figure 9). In another *in vitro* hMPO system reported by Kagan *et al.* [35], the degradation of IgG-coated oxidized SWCNTs seems to be much higher (solution turned translucent in 24 h), probably due to the constant higher concentrations of  $H_2O_2$  kept throughout their experiments by frequent (every 5 h) replenishment of hMPO and  $H_2O_2$ . We envision that by increasing the frequency and concentration of NADPH and MPO added, higher degradation efficiency of the *in vitro* enzymatic system would be achieved. Interestingly, based on the absorbance of  $S_2$  band, the 24 h degradation of ox-SWCNTs in untreated macrophages is very similar to that reported by Kagan *et al.* [35] (25.8% in this study *vs.* ~20%). Compared with ox-SWCNTs, 35% of OH-SWCNTs were degraded under the same condition, further confirming that OH-SWCNTs were more biodegradable than ox-SWCNTs. With PMA treatment, macrophages degraded up to 67% of ox-SWCNTs in 24 h (Figure 3F), which is comparable to the efficiency of neutrophils that were shown to degrade ~30% of ox-SWCNTs (no IgG coating) within 12 h [35], suggesting that through proper stimulation, the biodegradation of SWCNTs by macrophages would be elevated to that by neutrophils.

Taken together, we have demonstrated both ways of accelerating and slowing down the biodegradation of SWCNTs in macrophages by modulating the respiratory burst. In addition, SWCNTs

with defect sites were demonstrated to be more prone to be biodegraded by macrophages. Therefore, by careful functionalization of SWCNTs with proper coating that modulates the macrophage response, one can design better SWCNTs products with controlled retention time and toxicity. Alternatively, for drug delivery, modulating the biodegradation of nanocarriers may facilitate the release of the payloads as needed.

## 4. Materials and Methods

### 4.1. Materials

Pristine SWCNTs (p-SWCNTs, CNTs purity > 95%, SWCNT purity > 90%, ash < 5 weight %) and hydroxylated SWCNTs (OH-SWCNTs, purity > 90%) synthesized by chemical vapor deposition (CVD) method were originally obtained from Cheng du Organic Chemicals Co. (Cheng du, China). The following reagents were all purchased from Sigma (St. Louis, MO, USA): Phorbol myristate acetate (PMA), 2',7'-dichlorofluorescein diacetate (DCF-DA), ferricytochrome c,  $\beta$ -nicotinamide adenine dinucleotide 2'-phosphate reduced tetrasodium salt hydrate (NADPH), bovine erythrocyte superoxide dismutase (SOD), EGTA, Flavin adenine dinucleotide disodium salt hydrate (FAD), Myeloperoxidase (MPO), *N*-acetyl-L-cysteine (NAC).

### 4.2. Preparation of SWCNTs Solutions and Characterization

Acid-oxidized SWCNTs (ox-SWCNTs) were prepared according to the procedure described previously [65–67]. In detail, 10 mg of SWCNTs were suspended in 40 mL of a 3:1 mixture of concentrated H<sub>2</sub>SO<sub>4</sub>/HNO<sub>3</sub> in a 100 mL test tube and sonicated in a water bath (KQ-500DV, 100 kHz, 60%) for 24 h at 40–50 °C. The resultant suspension was then diluted with 200 mL deionized water and filtered through a membrane (pore size 0.22  $\mu$ m), followed by wash with 50 mL deionized water on the membrane. The acid-oxidized nanotubes were re-suspended in deionized water at a concentration of 1 mg/mL with brief sonication (KQ-50DE, 40 kHz, 2 min). The resultant ox-SWCNT suspension was black, well dispersed and had a neutral pH. The stock solutions of 1 mg/mL pristine SWCNTs (p-SWCNTs) and hydroxylated SWCNTs (OH-SWCNTs) were prepared separately by mixing SWCNTs with cell culture medium, followed by sonication for 5 min on ice using an ultrasonic probe tip sonicator (JY92-IIN, Ningbo Scientz Biotechnology Co., Ltd. Ningbo, China).

For transmission electron microscopy (TEM) characterization, SWCNTs were diluted to 0.01 mg/mL and precipitated onto a copper net and dried for imaging with a Hitachi H-7500 transmission electron microscopy at 80 kv (Tokyo, Japan). In addition, the infrared spectra of SWCNTs were collected by using a FT-IR spectrometer (JASCO, Inc., Easton, MD, USA). Raman spectroscopy analyses were performed on an inVia Raman spectroscopy (Renishaw Plc., Gloucestershire, UK) with a 633 nm wavelength laser source.

### 4.3. Cell Culture and Treatment

The murine monocytic cell line Raw264.7 was obtained from American Type Culture Collection (ATCC: TIB-71) and cultured in a humidified incubator with 95% air and 5% CO<sub>2</sub> at 37 °C in complete culture medium (cRPMI) containing RPMI-1640 fundamental medium and 100 U · mL<sup>-1</sup> penicillin/streptomycin, supplement with 10% heat deactivated fetal bovine serum (FBS). All ingredients for the media were purchased from Hyclone Inc. (Waltham, MA, USA). For optimization of respiratory burst induction in macrophages, cells were seeded in a 96-well plate at a density of 2 × 10<sup>5</sup> cells/mL and allowed to attach for overnight. Next, cells were loaded with 10  $\mu$ M of 2',7'-dichlorofluorescein diacetate (DCF-DA, a probe for intracellular ROS detection) at 37 °C for 30 min in dark. After wash with PBS twice, cells were treated with various concentrations (0–2  $\mu$ M) of phorbol myristate acetate (PMA, a respiratory burst inducer [51,68]), and the fluorescence of DCF in cells was measured on a Thermo Varioskan Flash microplate reader (Winooski, VT, USA) at the excitation/emission wavelength 488 nm/530 nm every 10 s for the first 90 min and at time points of

3, 6, 9, 12, and 24 h. To optimize the concentration of *N*-acetyl-L-cysteine (NAC) for the inhibition of respiratory burst, cells were first pretreated with various concentrations (0–5 mM) of NAC for 1 h and then loaded with DCF-DA. After, cells were treated by PMA (0.5  $\mu$ M) for 3 h in the presence of NAC (0–5 mM) and fluorescence detection was performed on the Varioskan Flash microplate reader. Furthermore, the DCF fluorescence in cells was also imaged with a Leica TCS SP5 confocal laser-scanning microscope (Mannheim, Germany) with a laser excitation at 488 nm and emission at 530 nm. For SWCNT treatment, cells ( $2 \times 10^5$  cells/mL) were seeded in culture dishes (60 mm in diameter) and allowed to attach for overnight. Then, 15  $\mu$ g of SWCNTs (p-SWCNTs, ox-SWCNTs, and OH-SWCNTs) were added to the cell culture along with PMA (0.5  $\mu$ M). Cells with NAC pretreatment (1 mM), followed by the addition of PMA (0.5  $\mu$ M) were set to investigate the inhibitory effect of antioxidant.

#### 4.4. Construction of *in Vitro* Respiratory Burst Enzymatic System and Verification

First, NADPH oxidase (NOX) was isolated according to the method described previously [54–56]. In detail, the macrophages were suspended to a concentration of  $0.5\text{--}1.5 \times 10^8$  cells/mL in a phosphate-sucrose buffer ( $1 \times$  PBS buffer, pH 7.0, and 340 mM sucrose). Cell disruption was performed by 5 min sonication using an ultrasonic probe tip sonicator (JY92-IIN, Ningbo Scientz Biotechnology Co., Ltd., Ningbo, China) in a 1.5 mL tube on ice. Then, the homogenate was centrifuged at  $800 \times g$  for 10 min at 4  $^{\circ}$ C to remove unbroken cells, nuclei, and large debris. The supernatant supplemented with EGTA (1 mM), and flavin adenine dinucleotide disodium salt hydrate (FAD, 0.1 mM) was used as the NADPH Oxidase (NOX). Thereafter, the second enzyme, SOD (300 U/mL) was added into the mixture, followed by the addition of NADPH (5 mM), NaCl (140 mM) and MPO (1 U). The full enzyme solution (total volume 500  $\mu$ L) was then incubated at 37  $^{\circ}$ C with shaking (80 rpm) and replenishment of MPO (1 U) and NADPH (40 mM) every 8 h in dark. For SWCNTs incubation, 8  $\mu$ g of SWCNTs per sample were mixed with the enzyme solution for indicated time, and then the samples were washed by centrifugation at 3400 rpm for 1 h twice and re-suspended in deionized water before Raman, UV-vis-NIR and TEM characterization.

The efficiency of this enzymatic system was evaluated by monitoring the generation of  $\text{O}_2^{\bullet-}$  and  $\text{H}_2\text{O}_2$  following the presence of NOX and SOD in the system, respectively.  $\text{O}_2^{\bullet-}$  was measured by the method of ferricytochrome c reduction, as described by Bellavite *et al.* [69]. In detail, the 60  $\mu$ L NOX solution were mixed with 0.94 mL phosphate-sucrose buffer containing ferricytochrome c (0.1 mM) and freshly prepared NADPH solution (0.2 mM). The absorption of ferrocyanochrome C, the product of ferricytochrome C reduction, was measured at 550 nm on a UV-visible spectrophotometer (Agilent 8453, Santa Clara, CA, USA). The  $\text{H}_2\text{O}_2$  was detected by using a Fluorimetric Hydrogen Peroxide Assay Kit (Sigma, St. Louis, MO, USA), according to manufacturer's instruction.

#### 4.5. Assessment of SWCNT Degradation

**Raman spectroscopy.** For cell samples, macrophages incubated with SWCNTs were fixed using 4% paraformaldehyde (4% PFA) onto a glass bottom cell culture dish (Nest Scientific, Rahway, NJ, USA). For samples from *in vitro* enzymatic system, 30  $\mu$ L of solution were dropped on a monocrystalline silicon wafer and allowed to dry overnight. An *inVia* Raman microscope spectrometer (Renishaw Plc., Gloucestershire, UK) with a 633 nm laser source was used for all samples, spectrum was obtained over the range of 800 to 1800  $\text{cm}^{-1}$  to visualize D and G band intensity changes throughout the degradation process. All Raman spectra were recorded for 10 s, 10% laser power, using a 50 L objective. For each sample, at least 20 spectra were recorded.

**Infrared spectroscopy (UV-vis-NIR).** For cell samples, macrophages incubated with SWCNTs were harvested together with the incubation medium. The cell suspensions were centrifuged (3400 rpm, 1 h) and resuspended in deionized water. Samples were further subjected to sonication for 20 min using an ultrasonic probe tip sonicator (JY92-IIN, Ningbo Scientz Biotechnology Co., Ltd. Zhejiang, China), and washed twice with PBS by centrifugation at 3400 rpm for 1 h to remove the cellular components

before assessment of SWCNT degradation. The UV-vis-NIR spectra were acquired by using a Cary 5000 UV-Vis-NIR spectrophotometer (Varian, Palo Alto, USA).

Transmission Electron Microscopy (TEM). SWCNTs were mixed with the enzyme solution for 24 h, and the samples then were washed by centrifugation at 3400 rpm for 1 h twice and resuspended in deionised water. Five  $\mu\text{L}$  of prepared sample were precipitated onto a copper net and dried for imaging with a Hitachi H-7500 transmission electron microscopy at 80 kv (Tokyo, Japan).

#### 4.6. Statistical Analysis

The data were expressed as the mean  $\pm$  S.D., and the difference between groups was evaluated using Student's *t*-test, with the significance level set at \*  $p < 0.05$  or \*\*  $p < 0.01$ .

### 5. Conclusions

In the present study, we explored and compared ways of modulating the biodegradation of three types of SWCNTs (p-, ox-, and OH-SWCNTs) in macrophages and in an *in vitro* enzymatic system simulating respiratory burst. The results demonstrated that: (1) SWCNTs carrying defect sites (ox-SWCNTs and OH-SWCNTs) could be degraded by macrophages, whereas p-SWCNTs were resistant to biodegradation probably due to the lack of reactive sites for oxidative attack; the order of degradation rate is OH-SWCNTs > ox-SWCNTs >> p-SWCNTs; (2) The biodegradation of SWCNTs could be significantly accelerated by PMA-activation in macrophages, or inhibited by an anti-oxidant, NAC; (3) Respiratory burst played an important role in accelerating the biodegradation of SWCNTs, as revealed by using the *in vitro* enzymatic system simulating respiratory burst. In addition, the *in vitro* enzymatic system constructed in the present study was proven to be able to simulate the enzymatic reaction cycles of respiratory burst for the effective degradation of SWCNTs. In principle, the enzymatic system can be expanded to study the degradation of other nanomaterials. Our findings on the biodegradation of functionalized SWCNTs would help to design safer SWCNT consumer products that are biodegradable and less toxic to living organisms, as well as drug carriers with controllable release of its payload. The ways of modulating the biodegradation of SWCNTs as we revealed might also provide invaluable clues on the development of intervention measurements for relieving the side effects of SWCNTs.

**Supplementary Materials:** Supplementary materials can be found at <http://www.mdpi.com/1422-0067/17/3/409/s1>.

**Acknowledgments:** The Chinese Academy of Sciences (XDB14040101) and the National Natural Science Foundation of China (21477146, 21277158, 91543203, 21321004, 21377142, and 21407168) supported this research.

**Author Contributions:** All authors read and approved the final manuscript. Bin Wan and Liang-Hong Guo conceived and designed the experiments; Jie Hou performed the experiments and analyzed the data; Yu Yang and Xiao-Min Ren contributed reagents/materials/analysis tools; Bin Wan and Jie Hou wrote the paper. Jing-Fu Liu helped with the Raman detection.

**Conflicts of Interest:** The authors declare no conflict of interest.

### Abbreviations

|                         |   |
|-------------------------|---|
| SWCNT                   | Single-walled carbon nanotube                               |
| HRP                     | Horse radish peroxidase                                     |
| MPO                     | Myeloperoxidase   |
| EPO                     | Eosinophil peroxidase                                       |
| NETs                    | Neutrophil extracellular traps                              |
| PMN                     | Polymorphonuclear neutrophils                               |
| $\text{O}_2^{\bullet-}$ | Superoxide anion  |
| NOX                     | Nicotinamide adenine dinucleotide phosphate (NADPH)-oxidase |

|            |   |
|------------|---|
| SOD        | Superoxide dismutase                              |
| PMA        | Phorbol myristate acetate                         |
| LPS        | Lipopolysaccharide                                |
| NAC        | N-acetyl-L-cysteine                               |
| ROS        | Reactive oxygen species                           |
| DCF-DA     | 2',7'-Dichlorofluorescein diacetate               |
| TEM        | Transmission electron microscopy                  |
| UV-vis-NIR | Ultraviolet-visible-near-infrared                 |
| FAD        | Flavin adenine dinucleotide disodium salt hydrate |

## References

- De Volder, M.F.L.; Tawfick, S.H.; Baughman, R.H.; Hart, A.J. Carbon nanotubes: Present and future commercial applications. *Science* **2013**, *339*, 535–539. [[CrossRef](#)] [[PubMed](#)]
- Marchesan, S.; Kostarelos, K.; Bianco, A.; Prato, M. The winding road for carbon nanotubes in nanomedicine. *Mater. Today* **2015**, *18*, 12–19. [[CrossRef](#)]
- Marchesan, S.; Melchionna, M.; Prato, M. Wire up on carbon nanostructures! How to play a winning game. *ACS Nano* **2015**, *9*, 9441–9450. [[CrossRef](#)] [[PubMed](#)]
- Karimi, M.; Solati, N.; Amiri, M.; Mirshekari, H.; Mohamed, E.; Taheri, M.; Hashemkhani, M.; Saeidi, A.; Estiar, M.A.; Kiani, P.; *et al.* Carbon nanotubes part I: Preparation of a novel and versatile drug-delivery vehicle. *Expert Opin. Drug Deliv.* **2015**, *12*, 1071–1087. [[CrossRef](#)] [[PubMed](#)]
- Martincic, M.; Tobias, G. Filled carbon nanotubes in biomedical imaging and drug delivery. *Expert Opin. Drug Deliv.* **2015**, *12*, 563–581. [[CrossRef](#)] [[PubMed](#)]
- Chen, X.; Kis, A.; Zettl, A.; Bertozzi, C.R. A cell nanoinjector based on carbon nanotubes. *Proc. Natl. Acad. Sci. USA* **2007**, *104*, 8218–8222. [[CrossRef](#)] [[PubMed](#)]
- Malarkey, E.B.; Parpura, V. Applications of carbon nanotubes in neurobiology. *Neurodegener. Dis.* **2007**, *4*, 292–299. [[CrossRef](#)] [[PubMed](#)]
- Karimi, M.; Solati, N.; Ghasemi, A.; Estiar, M.A.; Hashemkhani, M.; Kiani, P.; Mohamed, E.; Saeidi, A.; Taheri, M.; Avci, P.; *et al.* Carbon nanotubes part II: A remarkable carrier for drug and gene delivery. *Expert Opin. Drug Deliv.* **2015**, *12*, 1089–1105. [[CrossRef](#)] [[PubMed](#)]
- Prato, M.; Kostarelos, K.; Bianco, A. Functionalized carbon nanotubes in drug design and discovery. *Acc. Chem. Res.* **2008**, *41*, 60–68. [[CrossRef](#)] [[PubMed](#)]
- Wong, B.S.; Yoong, S.L.; Jagusiak, A.; Panczyk, T.; Ho, H.K.; Ang, W.H.; Pastorin, G. Carbon nanotubes for delivery of small molecule drugs. *Adv. Drug Deliv. Rev.* **2013**, *65*, 1964–2015. [[CrossRef](#)] [[PubMed](#)]
- Lamberti, M.; Zappavigna, S.; Sannolo, N.; Porto, S.; Caraglia, M. Advantages and risks of nanotechnologies in cancer patients and occupationally exposed workers. *Expert Opin. Drug Deliv.* **2014**, *11*, 1087–1101. [[CrossRef](#)] [[PubMed](#)]
- Schulte, P.A.; Kuempel, E.D.; Zumwalde, R.D.; Geraci, C.L.; Schubauer-Berigan, M.K.; Castranova, V.; Hodson, L.; Murashov, V.; Dahm, M.M.; Ellenbecker, M. Focused actions to protect carbon nanotube workers. *Am. J. Ind. Med.* **2012**, *55*, 395–411. [[CrossRef](#)] [[PubMed](#)]
- Maynard, A.D.; Kuempel, E.D. Airborne nanostructured particles and occupational health. *J. Nanopart. Res.* **2005**, *7*, 587–614. [[CrossRef](#)]
- Porter, A.E.; Gass, M.; Muller, K.; Skepper, J.N.; Midgley, P.A.; Welland, M. Direct imaging of single-walled carbon nanotubes in cells. *Nat. Nanotechnol.* **2007**, *2*, 713–717. [[CrossRef](#)] [[PubMed](#)]
- Tong, L.; Liu, Y.; Dolash, B.D.; Jung, Y.; Slipchenko, M.N.; Bergstrom, D.E.; Cheng, J.X. Label-free imaging of semiconducting and metallic carbon nanotubes in cells and mice using transient absorption microscopy. *Nat. Nanotechnol.* **2012**, *7*, 56–61. [[CrossRef](#)] [[PubMed](#)]
- Al-Jamal, K.T.; Nunes, A.; Methven, L.; Ali-Boucetta, H.; Li, S.; Toma, F.M.; Herrero, M.A.; Al-Jamal, W.T.; ten Eikelder, H.M.M.; Foster, J.; Mather, S.; Prato, M.; *et al.* Degree of chemical functionalization of carbon nanotubes determines tissue distribution and excretion profile. *Angew. Chem. Int. Ed.* **2012**, *51*, 6389–6393. [[CrossRef](#)] [[PubMed](#)]

17. Lam, C.W.; James, J.T.; McCluskey, R.; Hunter, R.L. Pulmonary toxicity of single-wall carbon nanotubes in mice 7 and 90 days after intratracheal instillation. *Toxicol. Sci.* **2004**, *77*, 126–134. [[CrossRef](#)] [[PubMed](#)]
18. Shi, X.H.; von dem Bussche, A.; Hurt, R.H.; Kane, A.B.; Gao, H.J. Cell entry of one-dimensional nanomaterials occurs by tip recognition and rotation. *Nat. Nanotechnol.* **2011**, *6*, 714–719. [[CrossRef](#)] [[PubMed](#)]
19. Jia, G.; Wang, H.F.; Yan, L.; Wang, X.; Pei, R.J.; Yan, T.; Zhao, Y.L.; Guo, X.B. Cytotoxicity of carbon nanomaterials: Single-wall nanotube, multi-wall nanotube, and fullerene. *Environ. Sci. Technol.* **2005**, *39*, 1378–1383. [[CrossRef](#)] [[PubMed](#)]
20. Magrez, A.; Kasas, S.; Salicio, V.; Pasquier, N.; Seo, J.W.; Celio, M.; Catsicas, S.; Schwaller, B.; Forro, L. Cellular toxicity of carbon-based nanomaterials. *Nano Lett.* **2006**, *6*, 1121–1125. [[CrossRef](#)] [[PubMed](#)]
21. Firme, C.P.; Bandaru, P.R. Toxicity issues in the application of carbon nanotubes to biological systems. *Nanomed. Nanotechnol. Biol. Med.* **2010**, *6*, 245–256. [[CrossRef](#)] [[PubMed](#)]
22. Warheit, D.B.; Laurence, B.R.; Reed, K.L.; Roach, D.H.; Reynolds, G.A.M.; Webb, T.R. Comparative pulmonary toxicity assessment of single-wall carbon nanotubes in rats. *Toxicol. Sci.* **2004**, *77*, 117–125. [[CrossRef](#)] [[PubMed](#)]
23. Shvedova, A.A.; Kisin, E.; Murray, A.R.; Johnson, V.J.; Gorelik, O.; Arepalli, S.; Hubbs, A.F.; Mercer, R.R.; Keohavong, P.; Sussman, N.; *et al.* Inhalation vs. aspiration of single-walled carbon nanotubes in C57BL/6 mice: Inflammation, fibrosis, oxidative stress, and mutagenesis. *Am. J. Physiol. Lung Cell. Mol. Physiol.* **2008**, *295*, L552–L565. [[CrossRef](#)] [[PubMed](#)]
24. Ali-Boucetta, H.; Nunes, A.; Sainz, R.; Herrero, M.A.; Tian, B.; Prato, M.; Bianco, A.; Kostarelos, K. Asbestos-like pathogenicity of long carbon nanotubes alleviated by chemical functionalization. *Angew. Chem. Int. Ed.* **2013**, *52*, 2274–2278. [[CrossRef](#)] [[PubMed](#)]
25. Kagan, V.E.; Tyurina, Y.Y.; Tyurin, V.A.; Konduru, N.V.; Potapovich, A.I.; Osipov, A.N.; Kisin, E.R.; Schwegler-Berry, D.; Mercer, R.; Castranova, V.; *et al.* Direct and indirect effects of single walled carbon nanotubes on raw 264.7 macrophages: Role of iron. *Toxicol. Lett.* **2006**, *165*, 88–100. [[CrossRef](#)] [[PubMed](#)]
26. Kisin, E.R.; Murray, A.R.; Keane, M.J.; Shi, X.C.; Schwegler-Berry, D.; Gorelik, O.; Arepalli, S.; Castranova, V.; Wallace, W.E.; Kagan, V.E.; *et al.* Single-walled carbon nanotubes: Geno- and cytotoxic effects in lung fibroblast v79 cells. *J. Toxicol. Environ. Health A* **2007**, *70*, 2071–2079. [[CrossRef](#)] [[PubMed](#)]
27. Jain, S.; Thakare, V.S.; Das, M.; Godugu, C.; Jain, A.K.; Mathur, R.; Chuttani, K.; Mishra, A.K. Toxicity of multiwalled carbon nanotubes with end defects critically depends on their functionalization density. *Chem. Res. Toxicol.* **2011**, *24*, 2028–2039. [[CrossRef](#)] [[PubMed](#)]
28. Ji, Z.; Zhang, D.; Li, L.; Shen, X.; Deng, X.; Dong, L.; Wu, M.; Liu, Y. The hepatotoxicity of multi-walled carbon nanotubes in mice. *Nanotechnology* **2009**, *20*. [[CrossRef](#)] [[PubMed](#)]
29. Sureshbabu, A.R.; Kurapati, R.; Russier, J.; Menard-Moyon, C.; Bartolini, I.; Meneghetti, M.; Kostarelos, K.; Bianco, A. Degradation-by-design: Surface modification with functional substrates that enhance the enzymatic degradation of carbon nanotubes. *Biomaterials* **2015**, *72*, 20–28. [[CrossRef](#)] [[PubMed](#)]
30. Kotchey, G.P.; Zhao, Y.; Kagan, V.E.; Star, A. Peroxidase-mediated biodegradation of carbon nanotubes *in vitro* and *in vivo*. *Adv. Drug Deliv. Rev.* **2013**, *65*, 1921–1932. [[CrossRef](#)] [[PubMed](#)]
31. Allen, B.L.; Kichambare, P.D.; Gou, P.; Vlasova, I.I.; Kapralov, A.A.; Konduru, N.; Kagan, V.E.; Star, A. Biodegradation of single-walled carbon nanotubes through enzymatic catalysis. *Nano Lett.* **2008**, *8*, 3899–3903. [[CrossRef](#)] [[PubMed](#)]
32. Allen, B.L.; Kotchey, G.P.; Chen, Y.; Yanamala, N.V.K.; Klein-Seetharaman, J.; Kagan, V.E.; Star, A. Mechanistic investigations of horseradish peroxidase-catalyzed degradation of single-walled carbon nanotubes. *J. Am. Chem. Soc.* **2009**, *131*, 17194–17205. [[CrossRef](#)] [[PubMed](#)]
33. Russier, J.; Menard-Moyon, C.; Venturelli, E.; Gravel, E.; Marcolongo, G.; Meneghetti, M.; Doris, E.; Bianco, A. Oxidative biodegradation of single- and multi-walled carbon nanotubes. *Nanoscale* **2011**, *3*, 893–896. [[CrossRef](#)] [[PubMed](#)]
34. Liu, X.Y.; Hurt, R.H.; Kane, A.B. Biodurability of single-walled carbon nanotubes depends on surface functionalization. *Carbon* **2010**, *48*, 1961–1969. [[CrossRef](#)] [[PubMed](#)]
35. Kagan, V.E.; Konduru, N.V.; Feng, W.; Allen, B.L.; Conroy, J.; Volkov, Y.; Vlasova, I.I.; Belikova, N.A.; Yanamala, N.; Kapralov, A.; *et al.* Carbon nanotubes degraded by neutrophil myeloperoxidase induce less pulmonary inflammation. *Nat. Nanotechnol.* **2010**, *5*, 354–359. [[CrossRef](#)] [[PubMed](#)]

36. Andon, F.T.; Kapralov, A.A.; Yanamala, N.; Feng, W.; Baygan, A.; Chambers, B.J.; Hultenby, K.; Ye, F.; Toprak, M.S.; Brandner, B.D.; *et al.* Biodegradation of single-walled carbon nanotubes by eosinophil peroxidase. *Small* **2013**, *9*, 2721–2729. [[CrossRef](#)] [[PubMed](#)]
37. Vlasova, I.I.; Sokolov, A.V.; Chekanov, A.V.; Kostevich, V.A.; Vasilyev, V.B. Myeloperoxidase-induced biodegradation of single-walled carbon nanotubes is mediated by hypochlorite. *Russ. J. Bioorg. Chem.* **2011**, *37*, 453–463. [[CrossRef](#)]
38. Chandrasekaran, G.; Choi, S.K.; Lee, Y.C.; Kim, G.J.; Shin, H.J. Oxidative biodegradation of single-walled carbon nanotubes by partially purified lignin peroxidase from *Sparassis latifolia* mushroom. *J. Ind. Eng. Chem.* **2013**, *20*, 3367–3374. [[CrossRef](#)]
39. Zhang, L.W.; Petersen, E.J.; Habteselassie, M.Y.; Mao, L.; Huang, Q.G. Degradation of multiwall carbon nanotubes by bacteria. *Environ. Pollut.* **2013**, *181*, 335–339. [[CrossRef](#)] [[PubMed](#)]
40. Farrera, C.; Bhattacharya, K.; Lazzaretto, B.; Andon, F.T.; Hultenby, K.; Kotchey, G.P.; Star, A.; Fadeel, B. Extracellular entrapment and degradation of single-walled carbon nanotubes. *Nanoscale* **2014**, *6*, 6974–6983. [[CrossRef](#)] [[PubMed](#)]
41. Teeguarden, J.G.; Webb-Robertson, B.J.; Waters, K.M.; Murray, A.R.; Kisin, E.R.; Varnum, S.M.; Jacobs, J.M.; Pounds, J.G.; Zanger, R.C.; Shvedova, A.A. Comparative proteomics and pulmonary toxicity of instilled single-walled carbon nanotubes, crocidolite asbestos, and ultrafine carbon black in mice. *Toxicol. Sci.* **2011**, *120*, 123–135. [[CrossRef](#)] [[PubMed](#)]
42. Elgrabli, D.; Floriani, M.; Abella-Gallart, S.; Meunier, L.; Gamez, C.; Delalain, P.; Rogerieux, F.; Boczkowski, J.; Lacroix, G. Biodistribution and clearance of instilled carbon nanotubes in rat lung. *Part. Fibre Toxicol.* **2008**, *5*. [[CrossRef](#)] [[PubMed](#)]
43. Nunes, A.; Bussy, C.; Gherardini, L.; Meneghetti, M.; Herrero, M.A.; Bianco, A.; Prato, M.; Pizzorusso, T.; Al-Jamal, K.T.; Kostarelos, K. *In vivo* degradation of functionalized carbon nanotubes after stereotactic administration in the brain cortex. *Nanomedicine* **2012**, *7*, 1485–1494. [[CrossRef](#)] [[PubMed](#)]
44. Babior, B.M.; Lambeth, J.D.; Nauseef, W. The neutrophil NADPH oxidase. *Arch. Biochem. Biophys.* **2002**, *397*, 342–344. [[CrossRef](#)] [[PubMed](#)]
45. Inoguchi, T.; Sonta, T.; Tsubouchi, H.; Etoh, T.; Kakimoto, M.; Sonoda, N.; Sato, N.; Sekiguchi, N.; Kobayashi, K.; Sumimoto, H.; *et al.* Protein kinase c-dependent increase in reactive oxygen species (ROS) production in vascular tissues of diabetes: Role of vascular NAD(P)H oxidase. *J. Am. Soc. Nephrol.* **2003**, *14*, S227–S232. [[CrossRef](#)] [[PubMed](#)]
46. Curulli, A.; Cesaro, S.N.; Coppe, A.; Silvestri, C.; Palleschi, G. Functionalization and dissolution of single-walled carbon nanotubes by chemical-physical and electrochemical treatments. *Microchim. Acta* **2006**, *152*, 225–232. [[CrossRef](#)]
47. Ahmad, M.N.; Xie, J.Y.; Ma, Y.H.; Yang, W.T. Surface functionalization of single-walled carbon nanotubes using photolysis for enhanced dispersion in an organic solvent. *New Carbon Mater.* **2010**, *25*, 134–140. [[CrossRef](#)]
48. Zhang, L.; Kiny, V.U.; Peng, H.Q.; Zhu, J.; Lobo, R.F.M.; Margrave, J.L.; Khabashesku, V.N. Sidewall functionalization of single-walled carbon nanotubes with hydroxyl group-terminated moieties. *Chem. Mater.* **2004**, *16*, 2055–2061. [[CrossRef](#)]
49. Octavia, Y.; Brunner-La Rocca, H.P.; Moens, A.L. NADPH oxidase-dependent oxidative stress in the failing heart: From pathogenic roles to therapeutic approach. *Free Radic. Biol. Med.* **2012**, *52*, 291–297. [[CrossRef](#)] [[PubMed](#)]
50. Morel, F.; Doussiere, J.; Vignais, P.V. The superoxide-generating oxidase of phagocytic-cells—Physiological, molecular and pathological aspects. *Eur. J. Biochem.* **1991**, *201*, 523–546. [[CrossRef](#)] [[PubMed](#)]
51. Green, S.P.; Phillips, W.A. Activation of the macrophage respiratory burst by phorbol-myristate acetate—Evidence for both tyrosine kinase-dependent and kinase-independent pathways. *Biochim. Biophys. Acta Mol. Cell Res.* **1994**, *1222*, 241–248. [[CrossRef](#)]
52. Decker, J.E.; Hight Walker, A.R.; Bosnick, K.; Clifford, C.A.; Dai, L.; Fagan, J.; Hooker, S.; Jakubek, Z.J.; Kingston, C.; Makar, J.; *et al.* Sample preparation protocols for realization of reproducible characterization of single-wall carbon nanotubes. *Metrologia* **2009**, *46*, 682–692. [[CrossRef](#)]
53. Hamon, M.A.; Itkis, M.E.; Niyogi, S.; Alvaraez, T.; Kuper, C.; Menon, M.; Haddon, R.C. Effect of rehybridization on the electronic structure of single-walled carbon nanotubes. *J. Am. Chem. Soc.* **2001**, *123*, 11292–11293. [[CrossRef](#)] [[PubMed](#)]

54. Bromberg, Y.; Pick, E. Activation of NADPH-dependent superoxide production in a cell-free system by sodium dodecyl-sulfate. *J. Biol. Chem.* **1985**, *260*, 3539–3545.
55. Green, T.R.; Schaefer, R.E. Intrinsic dichlorophenolindophenol reductase-activity associated with the superoxide-generating oxidoreductase of human-granulocytes. *Biochemistry* **1981**, *20*, 7483–7487. [[CrossRef](#)] [[PubMed](#)]
56. Gabig, T.G.; English, D.; Akard, L.P.; Schell, M.J. Regulation of neutrophil NADPH oxidase activation in a cell-free system by guanine nucleotides and fluoride. Evidence for participation of a pertussis and cholera toxin-insensitive G protein. *J. Biol. Chem.* **1987**, *262*, 1685–1690. [[PubMed](#)]
57. Babior, B.M. NADPH oxidase: An update. *Blood* **1999**, *93*, 1464–1476. [[PubMed](#)]
58. Nauseef, W.M. Nox enzymes in immune cells. *Semin. Immunopathol.* **2008**, *30*, 195–208. [[CrossRef](#)] [[PubMed](#)]
59. Bedard, K.; Krause, K.H. The nox family of ROS-generating NADPH oxidases: Physiology and pathophysiology. *Physiol. Rev.* **2007**, *87*, 245–313. [[CrossRef](#)] [[PubMed](#)]
60. Babior, B.M. NADPH oxidase. *Curr. Opin. Immunol* **2004**, *16*, 42–47. [[CrossRef](#)] [[PubMed](#)]
61. Kotchey, G.P.; Gaugler, J.A.; Kapralov, A.A.; Kagan, V.E.; Star, A. Effect of antioxidants on enzyme-catalysed biodegradation of carbon nanotubes. *J. Mat. Chem. B* **2013**, *1*, 302–309. [[CrossRef](#)] [[PubMed](#)]
62. Paravicini, T.M.; Touyz, R.M. NADPH oxidases, reactive oxygen species, and hypertension: Clinical implications and therapeutic possibilities. *Diabetes Care* **2008**, *31*, S170–S180. [[CrossRef](#)] [[PubMed](#)]
63. Kagan, V.E.; Kapralov, A.A.; St Croix, C.M.; Watkins, S.C.; Kisin, E.R.; Kotchey, G.P.; Balasubramanian, K.; Vlasova, I.I.; Yu, J.; Kim, K.; *et al.* Lung macrophages “digest” carbon nanotubes using a superoxide/peroxynitrite oxidative pathway. *ACS Nano* **2014**, *8*, 5610–5621. [[CrossRef](#)] [[PubMed](#)]
64. Zhao, Y.; Allen, B.L.; Star, A. Enzymatic degradation of multiwalled carbon nanotubes. *J. Phys. Chem. A* **2011**, *115*, 9536–9544. [[CrossRef](#)] [[PubMed](#)]
65. Liu, J.; Rinzler, A.G.; Dai, H.J.; Hafner, J.H.; Bradley, R.K.; Boul, P.J.; Lu, A.; Iverson, T.; Shelimov, K.; Huffman, C.B.; *et al.* Fullerene pipes. *Science* **1998**, *280*, 1253–1256. [[CrossRef](#)] [[PubMed](#)]
66. Dong, P.X.; Wan, B.; Guo, L.H. *In vitro* toxicity of acid-functionalized single-walled carbon nanotubes: Effects on murine macrophages and gene expression profiling. *Nanotoxicology* **2012**, *6*, 288–303. [[CrossRef](#)] [[PubMed](#)]
67. Wan, B.; Wang, Z.X.; Lv, Q.Y.; Dong, P.X.; Zhao, L.X.; Yang, Y.; Guo, L.H. Single-walled carbon nanotubes and graphene oxides induce autophagosome accumulation and lysosome impairment in primarily cultured murine peritoneal macrophages. *Toxicol. Lett.* **2013**, *221*, 118–127. [[CrossRef](#)] [[PubMed](#)]
68. Hu, T.H.; Liu, Z.X.; Shen, X. Roles of phospholipase D in phorbol myristate acetate-stimulated neutrophil respiratory burst. *J. Cell. Mol. Med.* **2011**, *15*, 647–653. [[CrossRef](#)] [[PubMed](#)]
69. Bellavite, P.; Berton, G.; Dri, P.; Soranzo, M.R. Enzymatic basis of the respiratory burst of guinea-pig resident peritoneal-macrophages. *J. Reticuloendothel. Soc.* **1981**, *29*, 47–60. [[PubMed](#)]

